

Tailoring Hierarchical Structure and Rare Earth Affinity of Compositionally Identical Polymers via Sequence Control

Peter A. Dykeman-Birmingham, Matthew P. Bogen, Supraja S. Chittari, Savannah F. Grizzard, Abigail S. Knight*

Department of Chemistry, The University of North Carolina at Chapel Hill, Chapel Hill, North Carolina 27599, United States

ABSTRACT: Macromolecule sequence, structure, and function are inherently intertwined. While well-established relationships exist in proteins, they are more challenging to define for synthetic polymer nanoparticles due to their molecular weight, sequence, and conformational dispersities. To explore the impact of sequence on nanoparticle structure, we synthesized a set of sixteen compositionally identical, sequence-controlled polymers with distinct monomer patterning of dimethyl acrylamide and a bioinspired, structure-driving di(phenylalanine) acrylamide (FF). Sequence control was achieved through multiblock polymerizations yielding unique ensembles of polymer sequences which were simulated by kinetic Monte Carlo simulations. Systematic analysis of global (tertiary- and quaternary-like) structure in this amphiphilic copolymer series revealed the effect of multiple sequence descriptors: the number of domains, the hydrophathy of terminal domains, and the patchiness (density) of FF within a domain, each of which impacted both chain collapse and the distribution of single- and multi-chain assemblies. Further, both the conformational freedom of chain segments and local-scale, β -sheet-like interactions were sensitive to the patchiness of FF. To connect sequence, structure, and a target function, we evaluated an additional series of nine sequence-controlled copolymers as sequestrants for rare earth elements (REEs) by incorporating a functional acrylic acid monomer into select polymer scaffolds. We identified key sequence variables that influence the binding affinity, capacity, and selectivity of polymers for REEs. Collectively, these results highlight the potential of and boundaries of sequence control via multiblock polymerizations to drive primary sequence ensembles, hierarchical structures, and ultimately modify the functionality of compositionally identical polymeric materials.

INTRODUCTION

Proteins are exemplary of the intricate relationship between the structure and function of macromolecules—precision folding governed by sequence patterning of amino acids enables efficient catalysts and receptors in complex aqueous environments.¹ The sophisticated capabilities of proteins have spurred efforts to translate their functionality into synthetic polymers, which offer expanded monomer chemistries and stability for use as enzyme mimics, multivalent therapeutics, and sequestrants for contaminants and valuable materials.²⁻⁴ Decades of synthetic development have enabled control over polymer primary structure, including composition, molecular weight, and monomer patterning.^{5,6} Additionally, the integration of structure at ligand-relevant length scales, akin to secondary structure, has been achieved with motifs incorporated into monomers: benzene-1,3,5-carboxamide that forms helical structures⁷ and di(phenylalanine) (FF) that elicits solvent segregated β -sheet-like interactions.^{8,9} However, the complex hierarchical structures of proteins have yet to be achieved with synthetic systems, which has limited their functional performance.

The use of polymer primary sequence as an independent variable to control the assembled structure is a nascent field; commonly, copolymers are synthesized as statistical distributions of monomers along the backbone and thereby are ensembles of disperse sequences.⁶ While strict

sequence-definition remains a challenge for most polymer classes, sequence control via macrocyclic ring opening,¹⁰ single unit molecular insertion,^{11,12} gradient,¹⁷ and multiblock polymerization¹³⁻¹⁶ are a synthetically tractable methods to dictate monomer patterning and approach the precision of biopolymers.^{6,18-20} Organization of polymer sequences into blocks or enriched in one or more monomers in this way resembles the domains of discrete secondary structures found in proteins. Theoretical,²¹ computational,²² and experimental^{17,23,24} investigations of these blocky copolymer systems have identified that this level of sequence control can both narrow and shift the size distributions of global polymer assemblies in dilute solution. Nevertheless, the degree of structural control that can be achieved with sequence patterning alone (e.g., how much can secondary-like structure or aggregation state be tuned using monomer patterning?) and threshold of dissimilarity in polymer sequences (e.g., how different must sequences be to observe differences in behavior?) remain uncertain. Appreciation and understanding of the structural impacts of reproducible sequence variables is key for designing functional polymeric materials.

Further, sequence control is a known strategy to improve the function of synthetic materials—as demonstrated with glycopolymers with increased binding capacity for lectins²⁵⁻²⁷ and oligomers with selective interactions for metal ions.^{21,22} An intriguing and societally pertinent application

for polymer functionality lies in the binding of rare earth elements (REEs), encompassing scandium, yttrium, and the lanthanum-lutetium series. These elements are critical to current and emerging technologies; yet, their isolation and separation present significant challenges due to chemical similarities across the ions and low concentrations in ores and recycled feedstocks.^{30,31} Proteins such as lanmodulin have demonstrated high affinity and selectivity for REEs using tailored arrangements of simple chelating moieties.³²⁻³⁴ While this illustrates the incredible capabilities of macromolecules, synthetic polymers offer further chemical and physical versatility. Pioneering studies employing readily scalable polymer sequestrates have demonstrated the importance of valency and hydrophobicity in facilitating high affinity binding to REEs.^{35,36} While polymeric materials offer tunable multivalent interactions, current designs lack the tailored structures required for substrate selectivity and affinity.^{2-4,37}

Drawing inspiration from biological systems, we sought to connect facets of polymer structure at multiple length scales. To achieve this, we leveraged multi-block polymerization, strategically biasing the location of monomers along the chain to generate ensembles of polymers that are a subset of a statistical polymer distribution featuring domains (i.e. patches) with higher frequencies of specific monomers.^{18,19,38} By synthesizing compositionally identical polymer ensembles with distinct monomer patterns, we established connections between monomer patterning and hierarchical polymer structure and further customized the selectivity and affinity for a model analyte - REEs in aqueous solution. This represents a significant stride towards emulating the precision hierarchical structures and binding observed in biological systems.

RESULTS AND DISCUSSION

Synthesis of sequence-controlled FF-DMA copolymers

To explore the role of polymer sequence in controlling hierarchical assembly, we synthesized a small library of sequence-controlled copolymers (SCPs) with the same composition: 23 wt% (~7 mol%) of the hydrophobic structure-forming di(phenylalanine)³⁹ (FF) monomer (Scheme S1 and Figures S1-3) and 77 wt% of hydrophilic dimethylacrylamide (DMA; ~15 kDa) using multi-block polymerization (Table 1 and Figure 1a). Guided by previous efforts with analogous statistical copolymers,⁹ we anticipated that this composition would lead to the formation of solvent segregated microstructures with β -sheet-like local interactions without compromising solubility in aqueous solution. Distinct soluble and structured domains were created along the polymer backbone via alternating block extensions of oligo(DMA) and oligo(FF-co-DMA) respectively. Using this method, each polymer synthesis generates a unique ensemble of sequences.

These SCP ensembles were categorized by three synthetically accessible sequence variables: the number of domains (3-8), the hydrophobicity of the terminal domains (0-2 terminal hydrophobic domains), and the patchiness of the structured domain (low, 40 wt% FF (~16mol%) in oligo(FF-co-DMA) blocks, to high, 60 wt% FF (~27 mol%)) (Figure 1b). As these SCP are compositionally identical, the total number of

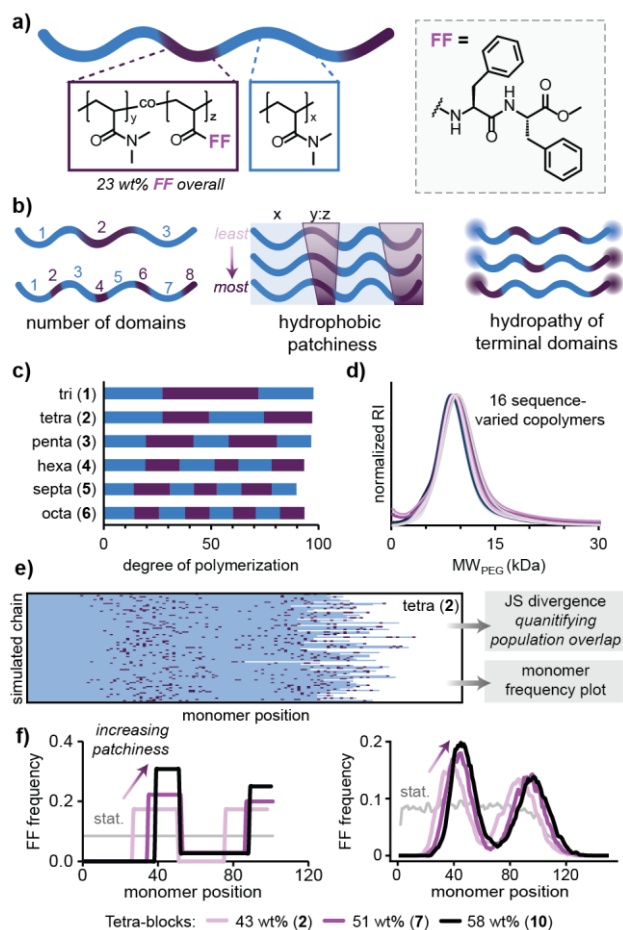


Figure 1. Sequence-controlled polymer library design. a) Schematic illustrating the composition of FF-DMA SCPs. b) Sequence variables considered in the copolymer library including the number of domains, the hydrophobic patchiness, and the hydrophobicity of terminal domains. c) Representative sequences (**1-6**) described by degrees of polymerization for DMA (blue) and FF-co-DMA (purple) segments, calculated by ¹H NMR. d) Overlay of organic phase SEC_{DMF} chromatograms for FF-DMA copolymers (**1-16**). The linear MW axis was calculated by converting SEC_{DMF} retention times using a PEG calibration curve (Figure S5). e) Subset of simulated sequences of tetra-block copolymers (**2**) containing DMA (blue) and FF (purple). f) FF monomer frequency distribution plots for tetra-block copolymers (**2**, **7**, **10**) and statistical copolymer (**16**) as calculated using ¹H NMR observed feed ratios (left) and calculated from kinetic Monte Carlo simulations (right, data smoothed with moving average of 3 points).

domains and the patchiness of the structured (i.e., FF-containing) domains necessarily dictate the domain lengths. To differentiate SCPs from a statistical copolymer, a lower bound of patchiness was selected as 40 wt% FF in the oligo(FF-co-DMA) block, and an upper bound at 60 wt% was selected to produce block segments large enough to be synthetically and analytically tractable. We hypothesized modifications to these variables, without varying the overall composition would provide access to assemblies with disparate local and global structures.

SCPs (**1-15**) were synthesized via iterative reversible addition-fragmentation transfer (RAFT) polymerizations to achieve blocky copolymers with controlled molecular weights and low Đ (Tables 1 and S1, Schemes S2-3).¹⁴ As ≥

<i>P</i> (#)	# blocks	<i>Mn</i> ^a (kDa)	<i>Mp</i> ^b (kDa)	\bar{D} ^b	wt% FF (total) ^a	wt% FF (block) ^c	# end FF blocks	JSD ^d	% collapse ^e	<i>R_h</i> ^e / <i>R_g</i> ^f	Porod
1	3 (tri)	14.8	8.8	1.09	24	43	0	0.19	25 (2.0)	0.76	3.5
2	4 (tetra)	15.2	8.7	1.13	23	43	1	0.10	32 (1.5)	0.90	3.3
3	5 (penta)	14.6	8.8	1.14	24	43	0	0.11	27 (0.9)	0.71	3.0
4	6 (hexa)	14.7	8.6	1.17	23	41	1	0.06	33 (1.1)	0.84	3.0
5	7 (septa)	13.8	8.3	1.16	24	40	0	0.08	30 (1.4)	0.75	2.9
6	8 (octa)	14.7	8.8	1.19	22	39	1	0.04	31 (2.1)	0.76	2.7
7	4 (tetra)	15.7	8.9	1.13	24	51	1	0.12	31 (3.2)	1.00	3.7
8	5 (penta)	16.5	9.2	1.13	24	52	0	0.14	26 (3.7)	0.97	3.8
9	6 (hexa)	16.7	9.4	1.16	23	52	1	0.07	32 (2.7)	0.85	3.2
10	4 (tetra)	16.0	8.9	1.14	23	58	1	0.12	30 (2.7)	1.18	4.0
11	5 (penta)	14.8	8.7	1.14	24	60	0	0.17	23 (2.2)	0.93	3.9
12	6 (hexa)	16.9	9.1	1.16	23	59	1	0.07	35 (6.4)	1.08	3.6
13	3 (tri)	16.6	9.1	1.11	23	43	2	0.18	39 (0.6)	1.08	3.4
14	4 (tetra)	15.4	8.9	1.13	23	43	1	0.13	31 (3.0)	0.98	3.1
15	5 (penta)	17.1	9.1	1.15	23	45	2	0.09	36 (1.4)	1.08	3.1
16	statistical	13.2	8.6	1.09	24	24	n.a.	0.00	35 (1.7)	0.57	2.6

Table 1. Characterization of FF-DMA copolymers. a) Calculated by ¹H NMR of purified polymers. b) Calculated as the average of three SEC chromatograms (DMF mobile phase). c) wt% FF in FF-co-DMA block calculated comparing ¹H NMRs pre- and post- polymerization reaction. d) Jensen-Shannon divergence of SCP sequence ensembles relative to statistical copolymer (16). Calculated using SEC in aqueous and DMF solvent systems. Values in parentheses are standard deviations of three replicates (Equation S2). e) *R_h* measured via DLS. f) Calculated by fitting SAXS scattering profiles to the exclude volume polymer model (Equation S1).

90% of the added monomer was consumed before subsequent block extension, leaving at most one monomer unincorporated, no intermediate purification steps were performed (Tables S2-4). With this method, controlled radical polymerizations were achieved with up to eight successive block extensions with Gaussian distributions and low dispersity ($\bar{D} < 1.3$), indicating high chain-end retention throughout the synthesis and good sequence control (Tables S5-7 and Figures S5-10). The composition of each block was monitored by ¹H NMR before and after extension reactions to track monomer incorporation into growing chains and confirm desired sequence variation between the polymers in the series (Figures 1c and S11-15). This synthetic strategy enabled the generation of polymers with unique sequence ensembles described by the sequence variables and is reproducible as demonstrated by the synthesis of both a replicated (**2r**; Figure S7, Tables S2 and S5) and inverted sequence (**14**; Tables S4 and S7). Following purification by precipitation in diethyl ether, analysis by ¹H NMR and organic phase size exclusion chromatography (SEC_{DMF}) confirmed the compositional similarity across the series of fifteen SCPs with varied sequence patterning (**1-15**) and one statistical copolymer (**16**) (Table 1, Figures 1d and S16).

To visualize and quantify the difference between the SCPs, the unique distributions of sequences were sampled by performing kinetic Monte Carlo simulations. We generated 1,000 chains for each SCP (**1-16**; Figures 1e and S17-20).⁴⁰⁻⁴² Each simulation incorporated experimental monomer conversions observed by NMR for each polymer synthesis and assumed statistical incorporation of FF and DMA as observed by NMR (Figure S15). Physical features of the polymerization including molecular weight (MW) and

compositional dispersity are found to be consistent within each SCP population, as all ensembles have similar MWs and are compositionally identical. Further, a plot of the calculated FF frequency at each sequence position illustrates differences between the unique SCP populations (Figure 1f).

While monomer patterning can be qualitatively compared between simulated populations of compositionally identical SCPs with a plot, differences between two SCPs can be quantified by Jensen-Shannon divergence (JSD). This parameter is bounded by one and zero corresponding to fully dissimilar and identical distributions respectively (Tables 1 and S8).^{43,44} The highest value obtainable would be that of a discrete sequence compared to a statistical population, which we calculated to be less than 1 (JSD = 0.79), providing a practical upper bound for the SCP series. The JSD values for the SCP ensembles (**1-15**) with reference to a statistical polymer distribution (**16**, the same composition as the SCPs) are correlated to the previously defined sequence variables (Table 1). Illustrated across SCPs **1-6**, JSD values generally decrease as the polymer chain is subdivided into more domains, indicating the SCPs more resemble a statistical copolymer and suggesting an upper limit to the possible number of sequence-controlled domains at this composition and MW (e.g., octa-block **6**, JSD = 0.04, Table 1). Further, as the size of hydrophobic domains are compressed to generate patchier SCPs (i.e. polymers with more dense FF domains), those ensembles of sequences diverge more from the statistical analogue (e.g., penta-blocks **3** and **11**, JSD = 0.11 and 0.16, Table 1). This quantitative comparison further demonstrates the diversity of sequence ensembles accessible with fixed composition (Tables 1 and S8).

Global structure of sequence-controlled FF-DMA copolymers

The sequence-dependent morphologies of SCP assemblies in aqueous solution were characterized by the ratio of the hydrodynamic radius (R_h , observed by dynamic light scattering; DLS) to the radius of gyration (R_g , observed by small angle X-ray scattering; SAXS; Figures S21-25, Table S9). This measure of compactness, R_h/R_g , is higher for globular proteins like BSA (~ 1.18 , Figure 2a)⁴⁵ and smaller for a random coil polymer in an ideal solvent (~ 0.65 , Figure 2a)⁴⁶. Interestingly, R_h/R_g values measured for these compositionally identical SCPs ranged from 0.71 – 1.18, suggesting the assemblies accessed by FF-DMA SCPs range from marginally collapsed to globular (Table 1, Figure 2a). The measured compactness of these assemblies increased with both the number of hydrophobic terminal blocks and FF patchiness. The R_h/R_g for the FF-DMA statistical copolymer (**16**) was 0.57, suggesting that the single-chain assembled into an ellipsoid-like shape, as has been observed for single-chain nanoparticles with BTA-driven local structures.^{7,47}

Analyses by SAXS and DLS were confounded by mixtures of single- and multi-chain assemblies; thus, we employed SEC, which resolves these populations, as a complementary descriptor of single-chain nanoparticle size. Statistical FF-DMA copolymers collapse to form single-chain assemblies,⁹ but the SCPs access distributions of multi- and single-chain assemblies in aqueous solution as a function of their sequence patterning (Figure 2). To quantify and compare the polymer radii in aqueous solution, the elution time of the single-chain species in a good solvent (SEC_{DMF}) and aqueous buffer (SEC_{aq}) were compared (Table S10). To provide a direct comparison between solvent systems, the ratios of molecular weights relative to PEG standards measured at peak maxima were calculated, termed percent collapse (Figure 2a, Equation S2, Table 1).^{9,48} Similar to values of R_h/R_g , the nanoparticle size measured by percent collapse of SCPs was observed to increase with the number of hydrophobic termini (Figure 2a). Compactness as measured by R_h/R_g increased as a function of patchiness, contrary to percent collapse, which remained constant as a function of patchiness for polymers with a single hydrophobic, FF-co-DMA, terminal block (**2, 4, 6, 7, 9, 10, 12**, and **14**) and decreased for polymers with two hydrophilic terminal blocks (**1, 3, 5, 8**, and **11**). We hypothesize this discrepancy in patchiness observed by R_h/R_g and percent collapse measured by SEC reflects increased particle compactness for multi-chain assemblies, as the calculation of percent collapse via SEC includes the peak molecular weight corresponding only to the single-chain population.

A comparison of the normalized SEC chromatograms further elucidated the population of multi-chain assemblies formed by the SCPs. The multi-chain assemblies ranged in molecular weights between 40-60 kDa, relative to PEG standards (Figures 2b-c and S26-28). While the distribution of multi- and single-chain assemblies varied as a function of flow rate, trends in the relative intensity of the multi-chain and single-chain assemblies were consistent at each flow rate, enabling qualitative comparisons of assembled polymer populations (Figure S29).

Blocky copolymers have previously been found to form multichain assemblies; this assembly was attributed to the

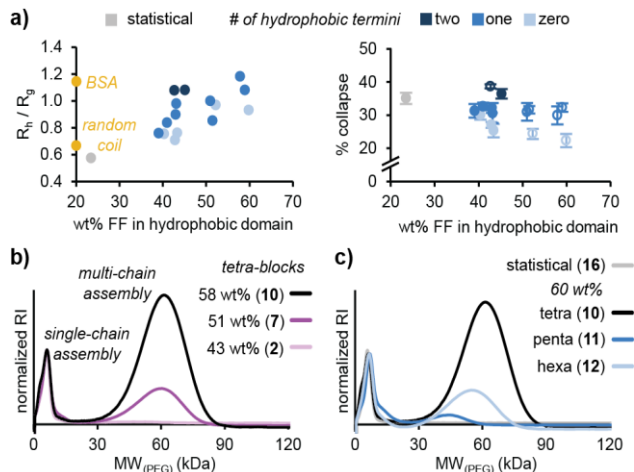


Figure 2. Characterization of FF-DMA copolymer global structure. a) R_h/R_g of copolymers (**1-16**) as a function of hydrophobic patchiness (left). Yellow circles highlight reported R_h/R_g values for BSA (top, 1.18) and random coil polymers (bottom, 0.65). Percent collapse of copolymers (**1-16**) as a function of hydrophobic patchiness (right). Error bars are the standard deviations of three replicates. Open circles indicate that multi-chain assemblies were observed but excluded from the present collapse calculation. SEC_{aq} chromatograms normalized to the intensity of the lower MW peak of c) tetra-block copolymers **2, 7**, and **10** with varying hydrophobic patchiness and d) tetra-, penta-, and hexa-block copolymers **10-12** each with ~ 60 wt% FF patchiness and statistical copolymer **16**. The calculation of the linear MW axis from SEC_{aq} retention time was performed using a PEG calibration curve (Figure S26).

higher entropic cost of intrachain collapse, thereby promoting intermolecular interactions.^{21,23,49} Consistent with that hypothesis, we observed by SEC_{aq} that the least patchy polymers (40 wt% FF, **1-6**) collapsed as single-chains while polymers with denser domains (50 and 60 wt% FF, **7** and **9-12**) resulted in the formation of the multi-chain assemblies. This suggests that an increase in FF density causes intramolecular folding to be more energetically demanding than intermolecular association (Figures 2b and S22,23). Corresponding trends of increased multi-chain populations with increased hydrophobic patchiness were observed by DLS as an increase in the average hydrodynamic radius (Table S9 and Figures S30-32).

Further, the population of multi-chain assemblies decreased with an increase in the number of domains across polymers for polymers with the same FF patchiness. For example, the multi-chain peak at approximately 60 kDa of the ~ 60 wt% tetra-block (**10**) constituted 33% of the integrated refractive index (RI) intensity by SEC_{aq}, whereas the analogous fraction for a hexa-block (**12**) with the same patchiness accounted for just 14% of the integrated RI (Figure 2c). We hypothesize that this decrease in multi-chain assembly results from the division of hydrophobic structured domains along the length of the polymer, therefore more evenly solvating the chain. Intersecting with the mitigating effect of block number on multichain assembly, fewer structured terminal domains also resulted in decreased multi-chain assembly by SEC_{aq}. For example, the multi-chain peak formed by the ~ 60 wt% penta-block (**11**), which has two hydrophilic oligo(DMA) terminal domains, accounted for

just 4% of the integrated RI peaks as compared to the 33% for the comparable tetra-block (**10**) and 14% for the hexa-block (**12**). We hypothesize that this reflects the entropic cost associated with shielding a hydrophobic terminal block from solvent relative to an analogous internal block. Finally, the same trends are observed for polymers with lower patchiness (~50 wt% FF, **7-9**) (Figure S28).

Each of the sequence variables defined herein were active in controlling both the global collapse and multi-chain assembly of SCPs providing multiple handles to tailor global structure.

Local structure of sequence-controlled FF-DMA copolymers

While global size and shape are important descriptors of polymer assemblies, local-scale interactions contributing to chain flexibility are similarly critical for complex functions.⁵⁰ We term flexibility as conformational freedom at the domain scale, akin to regions of disorder observed in proteins.⁵⁰ The flexibility of FF-DMA copolymers in dilute solution was assessed via SAXS.^{51,52} Transformation of the SAXS scattering profiles to $q^4 \cdot I(q)$ vs q^4 facilitates the assessment of polymer flexibility in terms of the Porod-Debye law, which predicts a decay in the scattering intensity proportional to q^{-4} for defined particles with smooth surfaces. Further, this transformation allows for fitting of the Porod exponent (Table 1 and S11).^{45,50} In this projection, collapsed and conformationally constrained polymers exhibit a characteristic plateau; whereas the scattering intensity of flexible polymers deviate from the Porod-Debye assumptions and the intensity continues rising as a function of q . The scattering profiles for all SCPs, except for the octa-block (**6**), indicated less flexibility than that of the statistical copolymer (**16**), highlighting the potential of sequence patterning to constrain polymer conformations (Figures 3a-b and S33-36). Between SCPs, flexibility was inversely proportional to FF patchiness (Figure 3a). This decrease in flexibility as a function of FF patchiness mirrored the increase in multi-chain assembly and compaction (R_h/R_g) as a function of the same variable. However, unlike multi-chain assembly and compaction, flexibility was minimally impacted by the number of domains and hydrophobic terminal domains (Figures 3b). We hypothesize that the repetition of self-similar domains along the backbone results in regions of comparable flexibility. Together these data indicate that while the flexibility of the polymers is connected to their collapsed/aggregated assembly, the two features are distinct.

The independence of sequence-based effects on global assembly and domain flexibility suggested that local structural features may also vary independently with sequence. To determine if sequence changes the β -sheet-like interactions between pendent FF moieties of SCPs, characteristic features of their circular dichroism (CD) spectra were compared. Consistent with previous reports of assembled FF, each spectrum exhibited two positive bands at ~198 and 219 nm, assigned to amide π - π^* and n - π^* transitions respectively.^{53,54} The positive band at 219 nm is congruous with rotational strength inherent to aromatic residues.⁵⁵ Notably, polymers with increased FF patchiness demonstrated a loss in ellipticity at 198 nm, indicating a change in local conformation of the FF interactions (Figures 3c and S37). To investigate the physical phenomena driving the ellipticity at

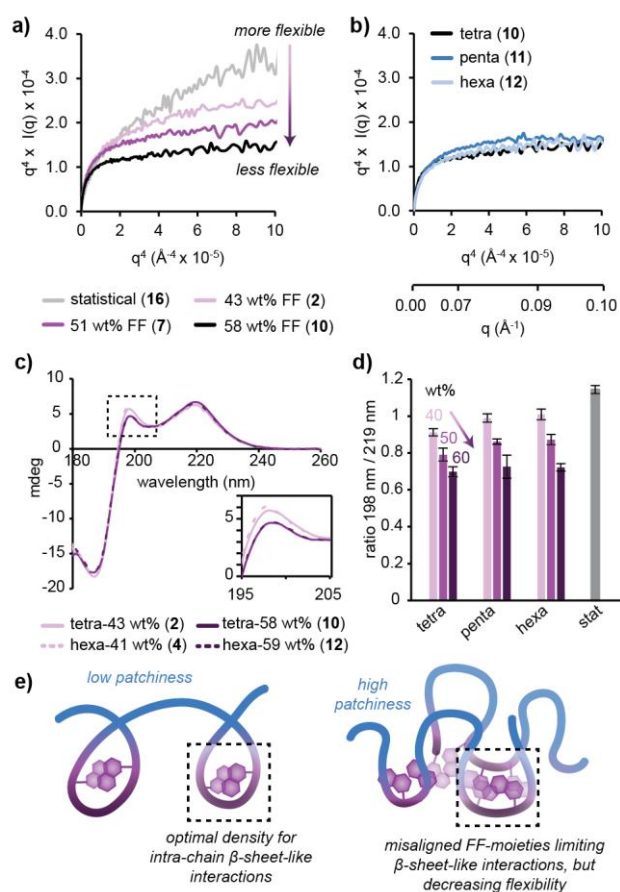


Figure 3. Flexibility and local structure of FF-DMA copolymers. Porod projection of SAXS scattering profiles for a) tetra-block copolymers **2**, **7**, and **10** with varying hydrophobic patchiness and statistical copolymer **16** and b) tetra-, penta-, and hexa-block copolymers **10-12** each with ~60 wt% FF patchiness. c) CD chromatograms of tetra- and hexa-block copolymers **2**, **4**, **10**, and **12**. Inset is an amplified view of local maxima at 198 nm. d) ratios of the CD maxima at 198 nm and 219 nm for tetra, penta, and hexa-block copolymers **2-4** and **7-12** and statistical copolymer **16**. Error bars are the standard deviations of three independent sample preparations. e) scheme depicting hypothesized relationship between polymer sequence and structure.

198 nm, hexafluoroisopropanol (HFIP) was titrated as a cosolvent to disrupt the β -sheet-like interactions formed by FF. As with previous observations of assembled and monomeric FF dipeptides,⁵³ the addition of HFIP (5 vol %) resulted in a loss of intensity of the 198 nm band and no changes in intensity of the 219 nm band, suggesting that the former uniquely reports on FF assembly (Figure S38). Further, subtracting the spectrum with HFIP from the corresponding spectrum in aqueous buffer suggests that the disrupted structure resembles that of an antiparallel β -sheet configuration dominated by a maximum at ~198 nm (Figure S38).⁵⁶⁻⁵⁸ Therefore, we hypothesize that the loss in ellipticity at 198 nm observed with increasing patchiness is due to a loss in β -sheet-like FF interactions.

To mitigate the effect of CD spectrum amplitude attributed to small variations in polymer concentration, the ratio of ellipticity at 198 nm and 219 nm was measured in triplicate. Calculating the ratio of 198 nm/219 nm ellipticity for a polymer at four concentrations spanning the dynamic range of

<i>P</i> (#)	# blocks	AA location	<i>M_n</i> (kDa)	wt% AA (total) ^a	wt% FF (total) ^a	wt% FF (block) ^a
17	4 (tetra)	soluble	11.7	19	24	38
18	4 (tetra)	soluble	12.3	19	23	45
19	5 (penta)	soluble	12.6	17	25	39
20	5 (penta)	soluble	12.9	17	24	47
21	4 (tetra)	structured	11.9	17	23	39
22	4 (tetra)	structured	12.6	16	23	45
23	5 (penta)	structured	12.8	17	25	38
24	5 (penta)	structured	12.7	16	24	46
25	statistical	n.a.	13.3	18	26	26

Table 2. Characterization of FF-AA-DMA copolymers. a) calculated by comparing 1H NMR pre- and post- block polymerization reactions.

CD detection corroborated that the ratio is invariant with respect to concentration (Figure S39). Further, this ratio is consistent between measurements of separately synthesized SCPs with the same sequence patterning (Figure S40). While a lower ratio of 198 nm / 219 nm strongly correlated with increasing patchiness, it only weakly correlated with the number of blocks, reminiscent of the variable dependence observed for flexibility (Figures 3d, S37, and Table S12). The concomitant loss in flexibility observed by SAXS and loss in β -sheet-like structure with increasing FF patchiness observed by CD suggest that the chain conformations accessible to these sequences struggle to form optimal β -sheet-like interactions and may explain the propensity of these chains to aggregate (Figure 3e).²¹ While all SCPs synthesized for this study showed a decrease in β -sheet-like interactions compared to the statistical copolymer (**16**; Figure 3d), we hypothesize that SCPs comprising different subsets of the statistical distribution could be designed with increased β -sheet-like interactions.

The local structure and flexibility of SCPs were uniquely controlled by changes to the patchiness of structured domains demonstrating that sequence control can be leveraged to tune polymer structure at this length scale in synthetic macromolecules.

REE binding by sequence-controlled FF-AA-DMA copolymers

With connections identified between sequence variables and polymer conformation at different length scales, we sought to further elucidate sequence-structure-function relationships of conformationally identical materials by targeting rare earth element (REE) binding. The selective sequestration of REEs from solution is not only a challenging and societally significant pursuit but also a sensitive model to explore the effect of sequence on function. To assess the impact of sequence on polymer affinity, capacity, and selectivity for REEs, we synthesized a second series of nine functional copolymers composed of FF, DMA, and a functional monomer, acrylic acid (AA), that differed only in sequence patterning (Table 2). Carboxylate functional groups, such as that of AA, have been shown to coordinate REE in biological³² and synthetic^{35,36} materials. Informed by the range of structures accessed by the sequence-controlled FF-DMA copolymers, the functional polymers varied in number of domains (4 and 5) and the FF patchiness in the hydrophobic domain (40 and 50 wt%) to access different degrees of β -

sheet-like interactions and global assemblies. Additionally, the location of AA, either within the soluble DMA segments or the structured FF-*co*-DMA domains, established a fourth sequence variable to augment polymer structure and binding characteristics (Figure 4a).

The functional sequence-controlled polymers (fSCPs) were synthesized using the aforementioned RAFT procedure with 26 wt% (30 DP, ~28 mol%) *tert*-butyl acrylate (*t*BA) as a pro-functional monomer (Figures S41-S46 and Table S13), allowing each polymer to bind 10 REEs in a hypothesized 1:3 (REE : AA) stoichiometry.³⁶ The pro-functional monomer facilitated statistical incorporation of FF, *t*BA, and DMA, and enabled the continued use of organic phase SEC_{DMF} to monitor block extension (Figure S47-48 and Table S14). Quantitative and selective deprotection of the pendent *tert*-butyl group with hydrochloric acid in HFIP and subsequent dialysis against nanopure water resulted in fSCPs with coordinating carboxylic acid groups (Figures S49-51).⁵⁹

We hypothesized that, like FF-DMA SCPs, the fSCPs would assemble to form sequence dependent global structures in the presence of REEs. The increased charge of the AA-containing polymers in the absence of REEs resulted in extended chains that were indistinguishable using SEC_{aq} and DLS (Figures 4b and S52-57). Upon incubation with terbium chloride [Tb(III)], a representative REE salt, polymer assemblies diverged. Polymers containing AA in the soluble domains (**17-20**) and the statistical polymer (**25**) visibly precipitated from solution upon the addition of Tb(III), convoluting structural characterization (Figure S58). The precipitation is mediated by the metal ions and is fully reversible with the addition of a competitive chelator (EDTA, Figure S59). For polymers with the AA in the structured domains (**21-24**), incubation with Tb(III) resulted in multi-chain assembly as observed by SEC_{aq}, though the precise ratio of metal to AA units was convoluted by dilution of the analytes on the column (Figures 4b). Stoichiometric titrations of Tb(III) into polymers with AA in the structured blocks (**21-24**) showed an increase in R_h by DLS until a Tb:AA ratio of 1:3 was reached (Figures S53-56). The size and solubility of the polymers was not further impacted by the number of blocks or the hydrophobic patchiness, in contrast to observations of FF-DMA SCPs, suggesting the significance of the binding interactions in driving global structure.

Unlike the global structure, FF-driven local structure was not disrupted by the presence of AA in the polymer chain as observed by CD in the absence of REEs. The inverse correlation observed between increased hydrophobic patchiness and β -sheet-like structure was consistent with observations from the FF-DMA SCP series (Figure S60). Stoichiometric titrations of Tb(III) into polymer solutions resulted in a decrease in the 198 nm / 219 nm ratio, suggesting that Tb binding reorganizes the β -sheet-like interactions formed by FF (Figures 4c and S60). For polymers with the AA in the structured domain (**21-24**), the local structure was not perturbed at ratios of Tb:AA above 1:3. A decrease in the 198 nm / 219 nm ratio was also observed for polymers with AA in the soluble domain, in addition to a decrease in overall signal corresponding to precipitation (Figure 4c).

Motivated by observations that Tb(III) binding reorganized polymer structure at multiple length scales, we sought to measure the affinity of those binding events to connect sequence, structure, and function. Polymer-Tb(III) affinities were compared in a competitive binding assay against a chelating dye, xylenol orange (XyO).^{60,61} An UV-Vis absorbance shift of the dye was observed between the Tb(III) bound and unbound states and measured relative to a standard curve of Tb:XyO solutions (Figure S61-62). Polymers (1 mM AA units in 40 mM MES, 100 mM KCl, pH 6) were incubated with Tb(III) (50 μ M TbCl₃) and an excess of XyO (60 μ M) to disfavor free Tb(III) in solution. While all polymers bound Tb(III) competitively with XyO, polymers with AA in the structured block showed a higher fraction of bound ions (> 33%; Figure 5a). No variation in binding affinity was observed between tetra- and penta-block copolymers; however, a compounding effect on binding affinity was observed with increased patchiness of the hydrophobic block. The fraction of bound Tb(III) exceeded 60% for the most patchy penta-block copolymer (46 wt% FF in FF-co-DMA-co-AA block, **24**). We hypothesize that the density of FF in the binding environment both increases the hydrophobicity of the pockets, desolvating the target ion, and facilitates the preorganization of binding sites. We note that the patchiness correlated with a decrease in β -sheet-like interactions, yet an increase in binding affinity for Tb(III), suggesting an induced-fit binding mechanism that is unable to maximize the formation of β -sheet-like interactions.

To estimate the binding affinity directly, polymer-Tb(III) solutions were analyzed using a luminescence resonance energy transfer (LRET) assay (Figures 5b and S63).⁶² Indirect excitation (255 nm) of Tb(III) via an energy transfer from an antennae conveniently provided by the FF moiety results in a characteristic, time-delayed emission at 545 nm. This emission is sensitive to the number of bound Tb(III) ions and their local environment including their proximity to FF.⁶³⁻⁶⁵ Polymer samples were incubated with Tb(III) in stoichiometric eq of zero to three relative to AA. As in SEC and CD experiments, precipitation of polymers with AA in the soluble block (**17-20**) and the statistical polymer (**25**) in the presence of Tb precluded measurement of luminescence. Binding curves were observed for polymers with AA in the structured block (**22-24**) and were fit to the Hill equation (Figure 5b and Table S15). While each of these polymers demonstrated mild binding cooperativity ($n \approx 1.3$) and comparable dissociation constants (apparent $K_{D,LRET} \approx 0.2$

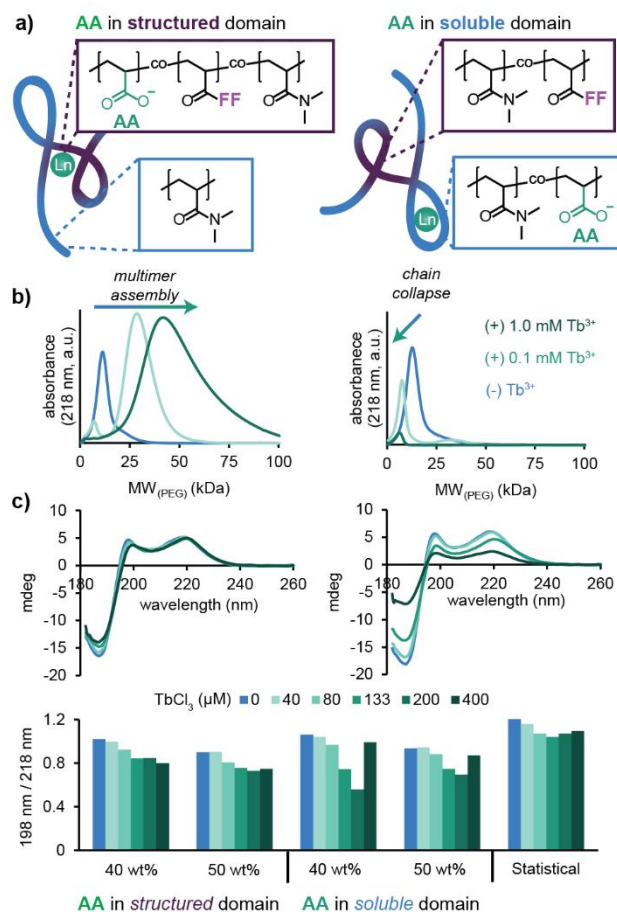


Figure 4. Structure of FF-AA-DMA sequence-controlled polymers unbound and bound to REEs. a) Schematic illustrating the location of the AA functional monomer in either the structured domain (FF-co-AA-co-DMA, left) or the soluble domain (DMA-co-AA, right). b) SEC_{aq} chromatograms of functional penta-block copolymers **24** (AA in structured domain, left) and **20** (AA in soluble domain, right) with 0 mM Tb(III) (blue), 0.1 mM Tb(III) (light green), and 1.0 mM Tb(III) (dark green). c) CD chromatograms of functional penta-block copolymers **24** (AA in structured domain, left) and **20** (AA in soluble domain, right) dissolved to AA concentration \approx 400 μ M. CD ratios of 198 nm to 219 nm for functional copolymers **17-25** in with varying quantities of Tb(III) (bottom).

mM), they differed predominantly in the magnitude of the observed luminescence response (B_{max}). The B_{max} was greatest for penta-blocks (**23** and **24**) and compounded by an increase in patchiness. The increase in LRET signal indicates an increase in the number of bound Tb(III) ions, binding events closer to FF, or fewer coordinating water molecules quenching the Tb(III) emission.^{62,63}

The absorbency of fSCPs (**20** and **22-25**) and a commercial ion exchange resin, Chelex 100 were compared after incubating with a 1:1:1 mol% mixture of lanthanum (LaCl₃ - La(III)), Tb(III), and gadolinium (GdCl₃ - Gd(III)) using a semi-permeable dialysis membrane (molecular weight cut-off of 8 kDa). After equilibrating the system for six hours, the metal concentrations of the dialysate were measured via inductively coupled plasma mass spectrometry (ICP-MS), and the depletion of metal was attributed to sequestration by the polymer. As Chelex 100 also uses pendent carboxylates for metal binding, it is a relevant and broadly accessible

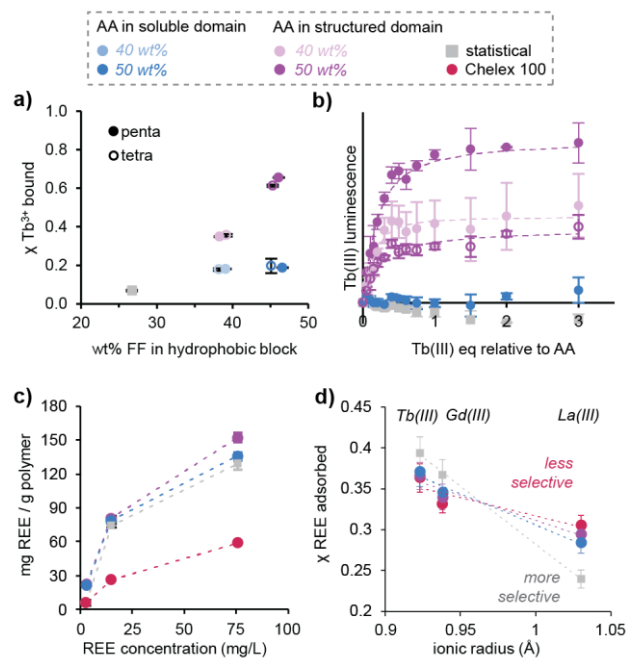


Figure 5. Characterization of REE binding by functional copolymers. a) Competitive binding of FF-AA-DMA copolymers (17-25, ~0.4 mg/mL) with xylene orange dye for Tb(III) measured as the fraction of Tb(III) stripped from the dye. b) LRET response of Tb(III) bound to ~0.4 mg/mL FF-AA-DMA copolymers 20-25 ($n \geq 3$). Binding of polymers 21-24 were fit to the Hill equation. c) REE binding capacity of polymers 20 (blue), 24 (purple), 25 (gray) and Chelex 100 resin (red) measured by ICP-MS. Dashed lines provided for clarity. d) Fraction of Tb(III) (0.92), Gd(III) (0.94) and La(III) (1.03) bound from a 1:1:1 mixture to FF-DMA-AA copolymers 20 (blue), 24 (purple), 25 (gray) and Chelex 100 resin (red). Lines are linear fits of the three points. Error bars are standard deviations of three

benchmark for comparison to fSCPs. Relative to the mass of the sequestrants, both functional statistical and fSCPs bound to the REEs more efficiently than Chelex 100 (Figure 5c and Table S16). This is likely due to the mass fraction of Chelex resin dedicated to crosslinking the material that did not participate in binding. Differences in binding capacity between statistical and fSCPs revealed that polymers with AA in the structured block bound the most total REEs, followed by those with AA in the soluble block, then the statistical copolymer. This trend mirrors the differences observed in polymer binding affinity to Tb(III) measured via a competition with XyO, suggesting that more carboxylic acids are bound to Tb(III) in the highest affinity polymers. Distinctions in polymer selectivity for individual REEs were observed by comparing the fraction of each ion bound from the ion mixture (Figure 5d, Table S14). While the polymers differed in the ratios of bound ions, they each favored binding to the heavy REEs as is commonly observed for REE chelators corresponding to increasing Lewis acidity.^{66,67} Notably, the statistical copolymer was observed to be the most selective of the series, followed by copolymers with AA in the soluble block, and finally those with AA in the structured block. As statistical copolymers comprise the full ensemble of sequences available to a given composition, these data suggest that within the full compositional ensemble are polymers with higher selectivity in addition to the lower selectivity SCs. Thus, these data demonstrate that sequence

control alone has a notable impact on target binding affinity. While the selected fSCPs exhibited a limited impact of sequence on selectivity and capacity, the results suggest further tunability can be achieved for the more complex aim of selectivity among chemically similar targets.

CONCLUSION

We have demonstrated the implementation of polymer sequence control via multiblock polymerization to tune both the hierarchical structure and function of synthetic materials, further bridging the gap between synthetic and biological polymers. The efficacy and bounds of this synthetic strategy to generate unique sequence ensembles was quantitatively described by Jensen-Shannon divergence calculations of sequence distributions generated with kinetic Monte Carlo simulations. Synthetic sequence variables describing the number, length, and composition of domains within compositionally identical copolymers were systematically varied to isolate the effects of monomer patterning on multi-chain assembly, single-chain collapse, flexibility, and local structure. In contrast, the local structure was tuned primarily by the patchiness of structured domains with a limited impact from additional sequence variables, enabling orthogonal control of hierarchical polymer structure. Further, we demonstrated the utility of sequence control to tune the affinity, capacity, and selectivity of model binding interactions by adapting this system to include a functional monomer. Particularly pronounced differences in affinity for REEs were observed between compositionally identical functional copolymers with varied patchiness of a hydrophobic structure-driving monomer. Diverse structures and tailored functions were achieved by biasing the patterning of monomers without the onerous requirements of strict sequence definition.

Continued interest in the development of polymeric materials with advanced functions including sensing, signaling and catalysis highlights the demand for strategies to control each element of hierarchical structure.⁶⁸ Though the focus of this study was on the separation of REEs, the versatility of this sequence based approach could be applied to develop polymeric materials for broad applications including the sequestration, transportation, and detection of a variety of analytes and pollutants, and the improvement and augmentation of enzyme-mimetic polymer catalysts. While this study used a small library of polymers to understand relationships between sequence, structure, and function in a defined system, studies with larger libraries will allow optimization for a target function and the identification of champion materials. The orthogonality of this approach to conventional compositional strategies makes a powerful combination for the development of the next generation of functional polymers.

ASSOCIATED CONTENT

Supporting information containing synthetic procedures, experimental details, and supplemental figures and tables including NMR, SEC, DLS, SAXS, CD and assay characterization is available. Software for kinetic Monte Carlo simulations and Jensen-Shannon divergence calculations are available at our GitHub.⁴²

AUTHOR INFORMATION

Corresponding Author

* * Abigail S. Knight (aknight@unc.edu)

ACKNOWLEDGMENT

This material is based upon work supported by the U.S. Department of Energy, Office of Science, Office of Basic Energy Sciences under Award Number DE-SC0021295. P.D.B. acknowledges support from the National Institute of General Medical Sciences of the National Institutes of Health under Award Number T32GM135122. S.S.C. acknowledges support from the National Science Foundation's Graduate Fellowship under Award Number DGE-2040435. We acknowledge the UNC Macromolecular Interactions Facility (CD and DLS; supported by the National Cancer Institute of the National Institutes of Health under award number P30CA016086), the UNC NMR Core Laboratory (supported by the National Science Foundation Award Number CHE-1828183), the UNC Biomarker Mass Spectrometry Facility (ICP-MS; supported by the Department of Environmental Science and Engineering at UNC-CH; National Science Foundation 2039788, 2001027, and 2304669, Environmental Protection Agency's Science to Achieve Results Program, and the National Institute of Environmental Health Sciences of the National Institutes of Health under Award number p30ES010126), the Lawrence laboratory (Spectromax plate reader) for assistance with instrumentation. We thank Dr. Zhixue Lu for valuable insight and discussions on the kinetic Monte Carlo simulations. Additionally, we thank Dr. Gregory Hura at the Advanced Light Source operated by Lawrence Berkeley National Laboratory on behalf of the Department of Energy, Office of Basic Energy Sciences through the Integrated Diffraction Analysis Technologies program supported by DOE office of Biological and Environmental research, the National Institutes of Health project ALS-ENABLE (P30 GM124169), and a High-End Instrumentation Grant S100D018483, for collection and consultation on SAXS characterization.

ABBREVIATIONS

AA, acrylic acid; SCP, sequence-controlled polymer; BTA, benzene-1,3,5-tricarboxamide; CD, circular dichroism; CTA, chain transfer agent; DLS, dynamic light scattering, DMA, dimethyl acrylamide; fSCP, functional sequence-controlled polymer; FF, di(phenylalanine); HFIP, hexafluoroisopropanol; LRET, luminescence resonance energy transfer; MW, molecular weight; RAFT, reversible addition-fragmentation transfer; REE, rare earth element; R_h , hydrodynamic radius; RI, refractive index; R_g , radius of gyration; SAXS, small angle x-ray scattering; SEC, size exclusion chromatography; UV-Vis, ultraviolet-visible

REFERENCES

(1) Dill, K. A.; Ozkan, S. B.; Shell, M. S.; Weikl, T. R. The Protein Folding Problem. *Annual review of biophysics* **2008**, *37*, 289. <https://doi.org/10.1146/ANNUREV.BIOPHYS.37.092707.153558>.
(2) Wijker, S.; Palmans, A. R. A. Protein-Inspired Control over Synthetic Polymer Folding for Structured Functional Nanoparticles in Water. *ChemPlusChem* **2023**, *88* (7), e202300260. <https://doi.org/10.1002/cplu.202300260>.
(3) Cole, J. P.; Hanlon, A. M.; Rodriguez, K. J.; Berda, E. B. Protein-like Structure and Activity in Synthetic Polymers. *Journal of Polymer Science Part A: Polymer Chemistry* **2017**, *55* (2), 191–206. <https://doi.org/10.1002/POLA.28378>.
(4) Barbee, M. H.; Wright, Z. M.; Allen, B. P.; Taylor, H. F.; Paterson, E. F.; Knight, A. S. Protein-Mimetic Self-Assembly with Synthetic Macromolecules. *Macromolecules* **2021**, *acs.macromol.0c02826*. <https://doi.org/10.1021/acs.macromol.0c02826>.

(5) Grubbs, R. B.; Grubbs, R. H. 50th Anniversary Perspective: Living Polymerization - Emphasizing the Molecule in Macromolecules. *Macromolecules* **2017**, *50* (18), 6979–6997. <https://doi.org/10.1021/acs.macromol.7b01440>.
(6) DeStefano, A. J.; Segalman, R. A.; Davidson, E. C. Where Biology and Traditional Polymers Meet: The Potential of Associating Sequence-Defined Polymers for Materials Science. *JACS Au* **2021**. <https://doi.org/10.1021/JACSAU.1C00297>.
(7) Stals, P. J. M.; Gillissen, M. A. J.; Paffen, T. F. E.; De Greef, T. F. A.; Lindner, P.; Meijer, E. W.; Palmans, A. R. A.; Voets, I. K. Folding Polymers with Pendant Hydrogen Bonding Motifs in Water: The Effect of Polymer Length and Concentration on the Shape and Size of Single-Chain Polymeric Nanoparticles. *Macromolecules* **2014**, *47* (9), 2947–2954. https://doi.org/10.1021/MA500273G/SUPPL_FILE/MA500273G_SI_001.PDF.
(8) Skaat, H.; Chen, R.; Grinberg, I.; Margel, S. Engineered Polymer Nanoparticles Containing Hydrophobic Dipeptide for Inhibition of Amyloid- β Fibrillation. *Biomacromolecules* **2012**, *13* (9), 2662–2670. <https://doi.org/10.1021/bm3011177>.
(9) Warren, J. L.; Dykeman-Bertingham, P. A.; Knight, A. S. Controlling Amphiphilic Polymer Folding beyond the Primary Structure with Protein-Mimetic Di(Phenylalanine). *Journal of the American Chemical Society* **2021**, *143* (33), 13228–13234. <https://doi.org/10.1021/JACS.1C05659>.
(10) Gutekunst, W. R.; Hawker, C. J. A General Approach to Sequence-Controlled Polymers Using Macrocyclic Ring Opening Metathesis Polymerization. *J. Am. Chem. Soc.* **2015**, *137* (25), 8038–8041. <https://doi.org/10.1021/jacs.5b04940>.
(11) Baker, J. G.; Zhang, R.; Figg, C. A. Installing a Single Monomer within Acrylic Polymers Using Photoredox Catalysis. *J. Am. Chem. Soc.* **2024**, *146* (1), 106–111. <https://doi.org/10.1021/jacs.3c12221>.
(12) Xu, J.; Fu, C.; Shanmugam, S.; Hawker, C. J.; Moad, G.; Boyer, C. Synthesis of Discrete Oligomers by Sequential PET-RAFT Single-Unit Monomer Insertion. *Angewandte Chemie International Edition* **2017**, *56* (29), 8376–8383. <https://doi.org/10.1002/anie.201610223>.
(13) Anastasaki, A.; Oschmann, B.; Willenbacher, J.; Melker, A.; Van Son, M. H. C.; Truong, N. P.; Schulze, M. W.; Discekici, E. H.; McGrath, A. J.; Davis, T. P.; Bates, C. M.; Hawker, C. J. One-Pot Synthesis of ABCDE Multiblock Copolymers with Hydrophobic, Hydrophilic, and Semi-Fluorinated Segments. *Angewandte Chemie International Edition* **2017**, *56* (46), 14483–14487. <https://doi.org/10.1002/ANIE.201707646>.
(14) Gody, G.; Maschmeyer, T.; Zetterlund, P. B.; Perrier, S. Pushing the Limit of the RAFT Process: Multiblock Copolymers by One-Pot Rapid Multiple Chain Extensions at Full Monomer Conversion. *Macromolecules* **2014**, *47* (10), 3451–3460. <https://doi.org/10.1021/MA402435N>.
(15) Benoit, D.; Hawker, C. J.; Huang, E. E.; Lin, Z.; Russell, T. P. One-Step Formation of Functionalized Block Copolymers. *Macromolecules* **2000**, *33* (5), 1505–1507. <https://doi.org/10.1021/ma991721p>.
(16) Antonopoulou, M.-N.; Whitfield, R.; Truong, N. P.; Wyers, D.; Harrison, S.; Junkers, T.; Anastasaki, A. Concurrent Control over Sequence and Dispersity in Multiblock Copolymers. *Nature Chemistry* **2021**, 1–9. <https://doi.org/10.1038/s41557-021-00818-8>.
(17) Ogura, Y.; Artar, M.; Palmans, A. R. A.; Sawamoto, M.; Meijer, E. W.; Terashima, T. Self-Assembly of Hydrogen-Bonding Gradient Copolymers: Sequence Control via Tandem Living Radical Polymerization with Transesterification. *Macromolecules* **2017**, *50* (8), 3215–3223. https://doi.org/10.1021/ACS.MACROMOL.7B00070/SUPPL_FILE/MA7B00070_SI_001.PDF.
(18) Lutz, J.-F. Defining the Field of Sequence-Controlled Polymers. *Macromolecular Rapid Communications* **2017**, *38* (24), 1700582. <https://doi.org/10.1002/marc.201700582>.

- (19) De Neve, J.; Haven, J. J.; Maes, L.; Junkers, T. Sequence-Definition from Controlled Polymerization: The next Generation of Materials. *Polym. Chem.* **2018**, *9* (38), 4692–4705. <https://doi.org/10.1039/C8PY01190G>.
- (20) Austin, M. J.; Rosales, A. M. Tunable Biomaterials from Synthetic, Sequence-Controlled Polymers. *Biomaterials Science* **2019**, *7* (2), 490–505. <https://doi.org/10.1039/C8BM01215F>.
- (21) Halperin, A. On the Collapse of Multiblock Copolymers Minimization of F with Respect to f Yields $Fe \sim NB4/\textcircled{R}$ and the Corresponding H, He \sim . *Macromolecules* **1991**, *24*, 1418–1419.
- (22) Patel, R. A.; Colmenares, S.; Webb, M. A. Sequence Patterning, Morphology, and Dispersity in Single-Chain Nanoparticles: Insights from Simulation and Machine Learning. *ACS Polym. Au* **2023**, *3* (3), 284–294. <https://doi.org/10.1021/acspolymersau.3c00007>.
- (23) Liu, R. C. W.; Pallier, A.; Brestaz, M.; Pantoustier, N.; Tribet, C. Impact of Polymer Microstructure on the Self-Assembly of Amphiphilic Polymers in Aqueous Solutions. *Macromolecules* **2007**, *40* (12), 4276–4286. https://doi.org/10.1021/MA070397S/SUPPL_FILE/MA070397SS120070214_114725.PDF.
- (24) Matsumoto, M.; Terashima, T.; Matsumoto, K.; Takenaka, M.; Sawamoto, M. Compartmentalization Technologies via Self-Assembly and Cross-Linking of Amphiphilic Random Block Copolymers in Water. *J. Am. Chem. Soc.* **2017**, *139* (21), 7164–7167. <https://doi.org/10.1021/jacs.7b03152>.
- (25) Gerke, C.; Ebbesen, M. F.; Jansen, D.; Boden, S.; Freichel, T.; Hartmann, L. Sequence-Controlled Glycopolymers via Step-Growth Polymerization of Precision Glycomacromolecules for Lectin Receptor Clustering. *Biomacromolecules* **2017**, *18* (3), 787–796. <https://doi.org/10.1021/acs.biomac.6b01657>.
- (26) Lavilla, C.; Yilmaz, G.; Uzunova, V.; Napier, R.; Becer, C. R.; Heise, A. Block-Sequence-Specific Glycopolypeptides with Selective Lectin Binding Properties. *Biomacromolecules* **2017**, *18* (6), 1928–1936. <https://doi.org/10.1021/acs.biomac.7b00356>.
- (27) Zhang, Q.; Collins, J.; Anastasaki, A.; Wallis, R.; Mitchell, D. A.; Becer, C. R.; Haddleton, D. M. Sequence-Controlled Multi-Block Glycopolymers to Inhibit DC-SIGN-Gp120 Binding. *Angewandte Chemie International Edition* **2013**, *52* (16), 4435–4439. <https://doi.org/10.1002/anie.201300068>.
- (28) Knight, A. S.; Zhou, E. Y.; Pelton, J. G.; Francis, M. B. Selective Chromium(VI) Ligands Identified Using Combinatorial Peptoid Libraries. *Journal of the American Chemical Society* **2013**, *135* (46), 17488–17493. <https://doi.org/10.1021/ja408788t>.
- (29) Lee, B.-C.; Chu, T. K.; Dill, K. A.; Zuckermann, R. N. Biomimetic Nanostructures: Creating a High-Affinity Zinc-Binding Site in a Folded Nonbiological Polymer. *J. Am. Chem. Soc.* **2008**, *130* (27), 8847–8855. <https://doi.org/10.1021/ja802125x>.
- (30) Sholl, D. S.; Lively, R. P. Seven Chemical Separations to Change the World. *Nature* **2016**, *532* (7600), 435–437. <https://doi.org/10.1038/532435a>.
- (31) Deng, B.; Wang, X.; Luong, D. X.; Carter, R. A.; Wang, Z.; Tomson, M. B.; Tour, J. M. Rare Earth Elements from Waste. *Science Advances* **2022**, *8* (6), eabm3132. <https://doi.org/10.1126/sciadv.abm3132>.
- (32) Mattocks, J. A.; Cotruvo, J. A. Biological, Biomolecular, and Bio-Inspired Strategies for Detection, Extraction, and Separations of Lanthanides and Actinides. *Chem. Soc. Rev.* **2020**, *49* (22), 8315–8334. <https://doi.org/10.1039/D0CS00653J>.
- (33) Cotruvo, J. A. Jr.; Featherston, E. R.; Mattocks, J. A.; Ho, J. V.; Laremore, T. N. Lanmodulin: A Highly Selective Lanthanide-Binding Protein from a Lanthanide-Utilizing Bacterium. *J. Am. Chem. Soc.* **2018**, *140* (44), 15056–15061. <https://doi.org/10.1021/jacs.8b09842>.
- (34) Mattocks, J. A.; Jung, J. J.; Lin, C.-Y.; Dong, Z.; Yennawar, N. H.; Featherston, E. R.; Kang-Yun, C. S.; Hamilton, T. A.; Park, D. M.; Boal, A. K.; Cotruvo, J. A. Enhanced Rare-Earth Separation with a Metal-Sensitive Lanmodulin Dimer. *Nature* **2023**, *618* (7963), 87–93. <https://doi.org/10.1038/s41586-023-05945-5>.
- (35) Archer, W. R.; Thompson, T. N.; Schulz, M. D.; Archer, W. R.; Thompson, T. N.; Schulz, M. D. Effect of Copolymer Structure on Rare-Earth-Element Chelation Thermodynamics. *Macromolecular Rapid Communications* **2021**, *42* (8), 2000614. <https://doi.org/10.1002/MARC.202000614>.
- (36) Archer, W. R.; Gallagher, C. M. B.; Vaissier Welborn, V.; Schulz, M. D. Exploring the Role of Polymer Hydrophobicity in Polymer–Metal Binding Thermodynamics. *Physical Chemistry Chemical Physics* **2022**, *24* (6), 3579–3585. <https://doi.org/10.1039/D1CP05263B>.
- (37) Archer, W. R.; Hall, B. A.; Thompson, T. N.; Wadsworth, O. J.; Schulz, M. D. Polymer Sequestrants for Biological and Environmental Applications. *Polymer International* **2019**, *68* (7), 1220–1237. <https://doi.org/10.1002/pi.5774>.
- (38) Lutz, J. F.; Lehn, J. M.; Meijer, E. W.; Matyjaszewski, K. From Precision Polymers to Complex Materials and Systems. *Nature Reviews Materials* **2016**, *1* (16024). <https://doi.org/10.1038/natrevmats.2016.24>.
- (39) Reches, M.; Gazit, E. Casting Metal Nanowires within Discrete Self-Assembled Peptide Nanotubes. *Science* **2003**, *300* (5619), 625–627. <https://doi.org/10.1126/science.1082387>.
- (40) Jayapurna, I.; Ruan, Z.; Eres, M.; Jalagam, P.; Jenkins, S.; Xu, T. Sequence Design of Random Heteropolymers as Protein Mimics. *Biomacromolecules* **2023**, *acs.biomac.2c01036*. <https://doi.org/10.1021/acs.biomac.2c01036>.
- (41) Smith, A. A. A.; Hall, A.; Wu, V.; Xu, T. Practical Prediction of Heteropolymer Composition and Drift. *ACS Macro Lett.* **2019**, *8* (1), 36–40. <https://doi.org/10.1021/acsmacrolett.8b00813>.
- (42) CopolymerSequenceGeneration. <https://github.com/UNC-Knight-Lab/CopolymerSequenceGeneration.jl>. (accessed-2024-01-10)
- (43) Gusev, L. V.; Vasilevskaya, V. V.; Makeev, V. Ju.; Khalatur, P. G.; Khokhlov, A. R. Segmentation of Heteropolymer Sequences Specifying Subsequences with Different Composition and Statistical Properties. *Macromolecular Theory and Simulations* **2003**, *12* (8), 604–613. <https://doi.org/10.1002/mats.200350024>.
- (44) Khokhlov, A. R.; Khalatur, P. G. Conformation-Dependent Sequence Design (Engineering) of AB Copolymers. *Physical Review Letters* **1999**, *82* (17), 3456–3459. <https://doi.org/10.1103/PhysRevLett.82.3456>.
- (45) Upadhyay, R.; Murthy, N. S.; Hoop, C. L.; Kosuri, S.; Nanda, V.; Kohn, J.; Baum, J.; Gormley, A. J. PET-RAFT and SAXS: High Throughput Tools to Study Compactness and Flexibility of Single-Chain Polymer Nanoparticles. *Macromolecules* **2019**, *52* (21), 8295–8304. <https://doi.org/10.1021/acs.macromol.9b01923>.
- (46) Balacescu, L.; Schrader, T. E.; Radulescu, A.; Zolnierczuk, P.; Holderer, O.; Pasini, S.; Fitter, J.; Stadler, A. M. Transition between Protein-like and Polymer-like Dynamic Behavior: Internal Friction in Unfolded Apomyoglobin Depends on Denaturing Conditions. *Scientific Reports* **2020**, *10*:1 **2020**, *10* (1), 1–11. <https://doi.org/10.1038/s41598-020-57775-4>.
- (47) Gillissen, M. A. J.; Terashima, T.; Meijer, E. W.; Palmans, A. R. A.; Voets, I. K. Sticky Supramolecular Grafts Stretch Single Polymer Chains. *Macromolecules* **2013**, *46* (10), 4120–4125. <https://doi.org/10.1021/MA4006846>.
- (48) Matsumoto, K.; Terashima, T.; Sugita, T.; Takenaka, M.; Sawamoto, M. Amphiphilic Random Copolymers with Hydrophobic/Hydrogen-Bonding Urea Pendants: Self-Folding Polymers in Aqueous and Organic Media. *Macromolecules* **2016**, *49* (20), 7917–7927. <https://doi.org/10.1021/acs.macromol.6b01702>.
- (49) Feng, Y.; Billon, L.; Grassl, B.; Bastiat, G.; Borisov, O.; François, J. Hydrophobically Associating Polyacrylamides and Their Partially Hydrolyzed Derivatives Prepared by Post-Modification. 2. Properties of Non-Hydrolyzed Polymers in Pure Water and Brine. *Polymer* **2005**, *46* (22), 9283–9295. <https://doi.org/10.1016/j.polymer.2005.07.054>.
- (50) Rambo, R. P.; Tainer, J. A. Characterizing Flexible and Intrinsically Unstructured Biological Macromolecules by SAS Using

- the Porod-Debye Law. *Biopolymers* **2011**, *95* (8), 559–571. <https://doi.org/10.1002/bip.21638>.
- (51) Dyer, K. N.; Hammel, M.; Rambo, R. P.; Tsutakawa, S. E.; Rodic, I.; Classen, S.; Tainer, J. A.; Hura, G. L. High-Throughput SAXS for the Characterization of Biomolecules in Solution: A Practical Approach. *Methods Mol Biol* **2014**, *1091*, 245–258. https://doi.org/10.1007/978-1-62703-691-7_18.
- (52) Hura, G. L.; Menon, A. L.; Hammel, M.; Rambo, R. P.; Poole, F. L.; Tsutakawa, S. E.; Jenney, F. E.; Classen, S.; Frankel, K. A.; Hopkins, R. C.; Yang, S.-J.; Scott, J. W.; Dillard, B. D.; Adams, M. W. W.; Tainer, J. A. Robust, High-Throughput Solution Structural Analyses by Small Angle X-Ray Scattering (SAXS). *Nat Methods* **2009**, *6* (8), 606–612. <https://doi.org/10.1038/nmeth.1353>.
- (53) Mishra, A.; Chauhan, V. S. Probing the Role of Aromaticity in the Design of Dipeptide Based Nanostructures. *Nanoscale* **2011**, *3* (3), 945–949. <https://doi.org/10.1039/c0nr00691b>.
- (54) Adler-Abramovich, L.; Reches, M.; Sedman, V. L.; Allen, S.; Tendler, S. J. B.; Gazit, E. Thermal and Chemical Stability of Diphenylalanine Peptide Nanotubes: Implications for Nanotechnological Applications. *Langmuir* **2006**, *22* (3), 1313–1320. <https://doi.org/10.1021/LA052409D>.
- (55) Woody, R. W. Aromatic Side-chain Contributions to the Far Ultraviolet Circular Dichroism of Peptides and Proteins. *Biopolymers* **1978**, *17* (6), 1451–1467. <https://doi.org/10.1002/BIP.1978.360170606>.
- (56) Sreerama, N. Structural Composition of betaI- and betaII-Proteins. *Protein Science* **2003**, *12* (2), 384–388. <https://doi.org/10.1110/ps.0235003>.
- (57) Balcerski, J. S.; Pysh, E. S.; Bonora, G. M.; Toniolo, C. Vacuum Ultraviolet Circular Dichroism of .Beta.-Forming Alkyl Oligopeptides. *J. Am. Chem. Soc.* **1976**, *98* (12), 3470–3473. <https://doi.org/10.1021/ja00428a013>.
- (58) Brahms, S.; Brahms, J.; Spach, G.; Brack, A. Identification of Beta,Beta-Turns and Unordered Conformations in Polypeptide Chains by Vacuum Ultraviolet Circular Dichroism. *Proc Natl Acad Sci U S A* **1977**, *74* (8), 3208–3212. <https://doi.org/10.1073/pnas.74.8.3208>.
- (59) Filippov, A. D.; Van Hees, I. A.; Fokkink, R.; Voets, I. K.; Kamperman, M. Rapid and Quantitative De- Tert-Butylation for Poly(Acrylic Acid) Block Copolymers and Influence on Relaxation of Thermoassociated Transient Networks. *Macromolecules* **2018**, *51* (20), 8316–8323. <https://doi.org/10.1021/acs.macromol.8b01440>.
- (60) Mattocks, J. A.; Tirsch, J. L.; Cotruvo, J. A. Chapter Two - Determination of Affinities of Lanthanide-Binding Proteins Using Chelator-Buffered Titrations. In *Methods in Enzymology*; Cotruvo, J. A., Ed.; Rare-Earth Element Biochemistry: Characterization and Applications of Lanthanide-Binding Biomolecules; Academic Press, 2021; Vol. 651, pp 23–61. <https://doi.org/10.1016/bs.mie.2021.01.044>.
- (61) Belleza, O. J. V.; Villaraza, A. J. L. Ion Charge Density Governs Selectivity in the Formation of Metal–Xylenol Orange (M–XO) Complexes. *Inorganic Chemistry Communications* **2014**, *47*, 87–92. <https://doi.org/10.1016/j.inoche.2014.07.024>.
- (62) Featherston, E. R.; Issertell, E. J.; Cotruvo, J. A. Probing Lanmodulin’s Lanthanide Recognition via Sensitized Luminescence Yields a Platform for Quantification of Terbium in Acid Mine Drainage. *Journal of the American Chemical Society* **2021**, *143* (35), 14287–14299. https://doi.org/10.1021/JACS.1C06360/SUPPL_FILE/JA1C06360_SI_001.PDF.
- (63) Hogue, C. W.; MacManus, J. P.; Banville, D.; Szabo, A. G. Comparison of Terbium (III) Luminescence Enhancement in Mutants of EF Hand Calcium Binding Proteins. *Journal of Biological Chemistry* **1992**, *267* (19), 13340–13347. [https://doi.org/10.1016/S0021-9258\(18\)42216-8](https://doi.org/10.1016/S0021-9258(18)42216-8).
- (64) Rabouan, S.; Delage, J.; Durand, W.; Prognon, P.; Barthes, D. Fluorescence Study of Some Terbium–Oligopeptide Complexes in Methanolic Solution. *Talanta* **2000**, *51* (4), 787–797. [https://doi.org/10.1016/S0039-9140\(99\)00353-7](https://doi.org/10.1016/S0039-9140(99)00353-7).
- (65) Ryu, J.; Lim, S. Y.; Park, C. B. Photoluminescent Peptide Nanotubes. *Advanced Materials* **2009**, *21* (16), 1577–1581. <https://doi.org/10.1002/adma.200802700>.
- (66) Archer, W. R.; Iftekhar, N.; Fiorito, A.; Winn, S. A.; Schulz, M. D. Synthesis of Phosphonated Polymer Resins for the Extraction of Rare-Earth Elements. *ACS Applied Polymer Materials* **2022**. <https://doi.org/10.1021/ACSAPM.1C01813>.
- (67) Cheisson, T.; Schelter, E. J. Rare Earth Elements: Mendeleev’s Bane, Modern Marvels. *Science* **2019**, *363* (6426), 489–493. <https://doi.org/10.1126/science.aau7628>.
- (68) Verde-Sesto, E.; Arbe, A.; Moreno, A. J.; Cangialosi, D.; Alegría, A.; Colmenero, J.; Pomposo, J. A. Single-Chain Nanoparticles: Opportunities Provided by Internal and External Confinement. *Materials Horizons* **2020**, *7* (9), 2292–2313. <https://doi.org/10.1039/D0MH00846J>.

Insert Table of Contents artwork here

